Nanoscale

PAPER

View Article Online
View Journal | View Issue

Cite this: *Nanoscale*, 2018, **10**, 16184

High-performance, color-tunable fiber shaped organic light-emitting diodes†

Keum-Jin Ko, ‡[a] Hock Beng Lee, ‡[a] Hyun Myung Kim,[b] Gil Ju Lee,[b] So-Ra Shin,[a] Neetesh Kumar,[a] Young Min Song *[b] and Jae-Wook Kang *[a]

Received 25th June 2018,
Accepted 12th August 2018

DOI: 10.1039/c8nr05120h

rsc.li/nanoscale

In recent years, extensive research has been undertaken to develop fiber-shaped optoelectronic devices, because they are aesthetically pleasing, light in weight, and exhibit superior light emitting properties when compared with conventional planar analogues. In this work, we have successfully developed hollow-fiber shaped organic light emitting diodes (HF-OLED) with an exceptionally high luminance and facile color tunability. The HF-OLED device was fabricated by hierarchically depositing amorphous indium-doped tin oxide electrode on a hollow-fiber, followed by the sequential deposition of light-emitting organic layers and Al cathode. The external quantum efficiency of the HF-OLED is more than ~2.0 times higher than that of a planar-OLED. The experimental results are in good agreement with the output of optical simulations, revealing that the use of a hollow-fiber has contributed to a ~2.3 times improvement in light extraction efficiency. Furthermore, the color emission of a single HF-OLED device could be easily tuned from a green to yellowish-green wavelength after the injection of a super-yellow solution. The novel color tunable nature of the HF-OLED further broadens its application in the field of modern lighting and display technology.

Introduction

Organic light emitting diodes (OLEDs) are generally considered the most popular optoelectronic device in the modern lighting and large-area display markets because of their unique features such as light weight, great mechanical flexibility, large viewing angle, high optical transparency, and color-purity.[1,2] In recent years, there has been growing research interest in developing fiber-shaped optoelectronic devices, including fiber-based photodetectors,[3] surface emitting fiber-lasers,[4] fiber-based dye sensitized solar cells,[5] electrochemical cells,[6] as well as fiber-OLEDs.[7,8] Based on the described advantages, these fiber-based electronics hold great promise for use in portable and wearable electronics, and fiber geometries are frequently modified to meet the specific requirements of final applications. Hollow-fibers (HFs) have been designed and widely applied in lighting technology fields, from the fabrication of integrated light sources to low cost solid-state lighting, including OLEDs.[9]

For an OLED application, it is extremely important for the substrate/electrode material to possess optical transparency, electrical conductivity, and thermal stability, *i.e.* factors which optimize the fabrication cost, efficiency, and lifetime of the device. As is commonly known, conventional planar-OLED devices generally suffer from light extraction issues, whereby only a mere 20% of the generated light can be extracted from the device as useable light. This tremendously hinders planar-OLED performance and light emitting efficiency.[10,11] A number of approaches have been implemented to improve the efficiency of planar-OLED devices, such as introducing additional light extraction structures,[11–14] allocation of Bragg scattering effects,[15] and substrate modifications,[16] and thermally activated delayed fluorescent (TADF).[17–19] Inevitably, all of these approaches involve the use of a third-party medium in the planar-OLED device architecture and there is no benchmark in comparing the enhancement efficiency. In the previous literature, the use of a fiber-based substrate in OLED application has been demonstrated.[6–9,20] The most noticeable difference between fiber-based OLEDs and conventional OLEDs comes in their shape and appearance, in which fiber-based OLEDs typically exhibit a cylindrical geometry. Herein, we demonstrate the unprecedented use of a cylindrically-shaped fiber with a hollow-core (abbreviated as hollow-fiber henceforth) for OLED device applications. Unlike the typical

[a]*Department of Flexible and Printable Electronics, Polymer Materials Fusion Research Center, Chonbuk National University, Jeonju 54896, Republic of Korea. E-mail: jwkang@jbnu.ac.kr*
[b]*School of Electrical Engineering and Computer Science, Gwangju Institute of Science and Technology, Gwangju 61005, Republic of Korea. E-mail: ymsong@gist.ac.kr*

†Electronic supplementary information (ESI) available. See DOI: 10.1039/c8nr05120h

‡These authors are made equal contribution to this paper.

fiber substrate, a hollow-fiber has an empty core to accommodate different colored solutions and scattering effect materials, which is an exceptionally useful feature in color-tunable lighting applications. Furthermore, the cylindrical geometry of the hollow-fiber can effectively suppress the wave-guided light loss at the electrode/substrate interface, thus contributing to a greater luminance efficiency (LE). In addition, the use of hollow-fibers could circumvent the use of additional internal and external light extraction structures, as commonly practiced in planar OLEDs. This grants hollow-fiber-based OLEDs (HF-OLEDs) a huge advantage over planar OLEDs as far as the commercialization cost of the product is concerned. The cylindrical geometry of HF-OLED makes it possible for the wave-guides to be used in wearable device applications.

Despite the increasing popularity of fiber-shaped OLEDs in lighting applications, there is a relative insufficiency of scientific literature exploring the impact that the fiber geometry (especially hollow-fiber) exerts on the device performance of the OLED. Therefore, in this work, we emphasized investigation into the positive effects of fiber-based OLEDs that arise from non-planar device geometries. To provide a concise study, we compared the device performance of HF-OLEDs with conventional planar OLEDs. HF-OLEDs exhibited a superior device performance than that of planar OLEDs, evidenced by their considerably higher maximum luminance, luminance efficiency, and external quantum efficiency (EQE). Theoretical simulations also reveal that the circular geometry of HF-OLEDs was more effective in reducing substrate modes and wave-guide modes as a light-loss mechanism than the planar geometry of conventional OLEDs, resulting in significantly enhanced light extraction efficiency. Furthermore, the as-fabricated HF-OLED also displayed a promising color-tunable nature after the insertion of different colored solutions. HF-OLEDs can serve as a promising alternative to conventional OLED devices in the field of modern lighting.

Experimental methods

Fabrication of HF-electrode

First, glass substrates were successively sonicated in acetone, ethanol, and boiled in isopropyl alcohol (IPA) for 5 min. The glass substrates were then dried in a laboratory oven at 120 °C for 30 min. The elastomeric polydimethylsiloxane (PDMS) and curing agent (Sylgard-184, Dow Corning. Co, Korea) solution was then spin-coated onto the glass substrates at 600 rpm for 40 s to yield a thickness of ~150 μm. Next, soda lime glass plain hollow-fibers (#2502, Kimble & Chase, Korea) were attached on the PDMS film template and thermally cured in the oven at 100 °C for 30 min. This process was followed by the deposition of a ~150 nm-thick amorphous indium-doped tin oxide (a-ITO) anode layer onto the hollow-fiber *via* an ultra-high vacuum (1.0×10^{-7} torr) sputtering system (A-Tech System). The a-ITO deposition process was performed at a sputtering power of 100 W for 10 min, under a working pressure of 1.0×10^{-3} torr ($Ar : O_2$ ratio = 40 : 0.2).

Fabrication of the HF-OLED

Bottom emission OLED devices were fabricated on the as-prepared HF-electrode. Prior to the deposition of the organic active layers, the HF-electrode embedded substrates were UV/ozone treated for 900 s. The organic active layers of the HF-OLED consisted of three primary organic materials: ~100 nm-thick 4,4′,4′-tris[2-naphthyl(phenyl)amino]triphenylamine (2-TNATA) as a hole injection layer, ~20 nm-thick *N*,*N*′-bis(naphthalen-1-yl)-*N*,*N*′-bis(phenyl)benzidine (NPB) as a hole transporting layer and ~60 nm-thick tris-(8-hydroxyquinoline)aluminium (Alq_3) as a light-emitting layer. These layers were thermally evaporated onto the as-prepared HF-electrodes at an evaporation rate of 0.4–0.7 Å s^{-1}. To complete device fabrication, a ~0.5 nm-thick lithium fluoride (LiF) and ~150 nm-thick aluminium (Al) cathode were thermally evaporated onto the active layer at an evaporation rate of 0.1 Å s^{-1} and 4–5 Å s^{-1}, respectively. The schematic fabrication process and the device architecture of the HF-OLED are illustrated in Fig. 1 whereas the refractive index (n) values of glass, a-ITO and combined organic layers of planar- and HF-OLED can be found in Fig. S1 in ESI.†

Characterization of HF-electrode and HF-OLED

Surface morphology and 3-D imaging of the HF-electrodes at different angles was conducted using a field-emission scanning electron microscope (FE-SEM, Hitachi S-4800). The sheet resistance (R_{sheet}) and optical transmittance (T) of the a-ITO electrode at different thicknesses were measured using a non-contact resistance measurement instrument (Napson, EC-80P) and an UV-vis spectrophotometer (PerkinElmer Lambda 750), respectively. For device characterization, the current density–voltage–luminance (J–V–L) characteristics, EQE, electroluminescence (EL) spectra, international commission on illumination (CIE) coordinates, and angle-resolved EL intensity of HF-OLEDs were measured using a source measure unit (Keithley 236) and a spectroradiometer (Konta Minolta CS-2000) with a close-up lens (CS A35) under ambient air. For CS-2000 spectroradiometer measurements, the diameter of the measurement spot is Ø 0.5 mm (without close-up lens) and Ø 0.1 mm (with close-up lens). The area of the emitting cells (A) was calculated using equation below:

$$A = \pi \times r \times L$$

where r and L represents the radius of the hollow-fiber and length of the emitting cell, respectively. The detailed experimental setup for CS-2000 spectroradiometer measurement is illustrated in Fig. S3.†

Theoretical simulation of HF-OLEDs

For the navigation of light rays from the substrate to the air in an HF-OLED device with geometrical considerations, full trans-scale 3D optical simulations, based on the Monte Carlo method, were carried out using commercial software (ZEMAX Optic Studio, Radiant Zemax LLC, USA).[21] The ray-tracing simulation results provided the extraction efficiency, out-

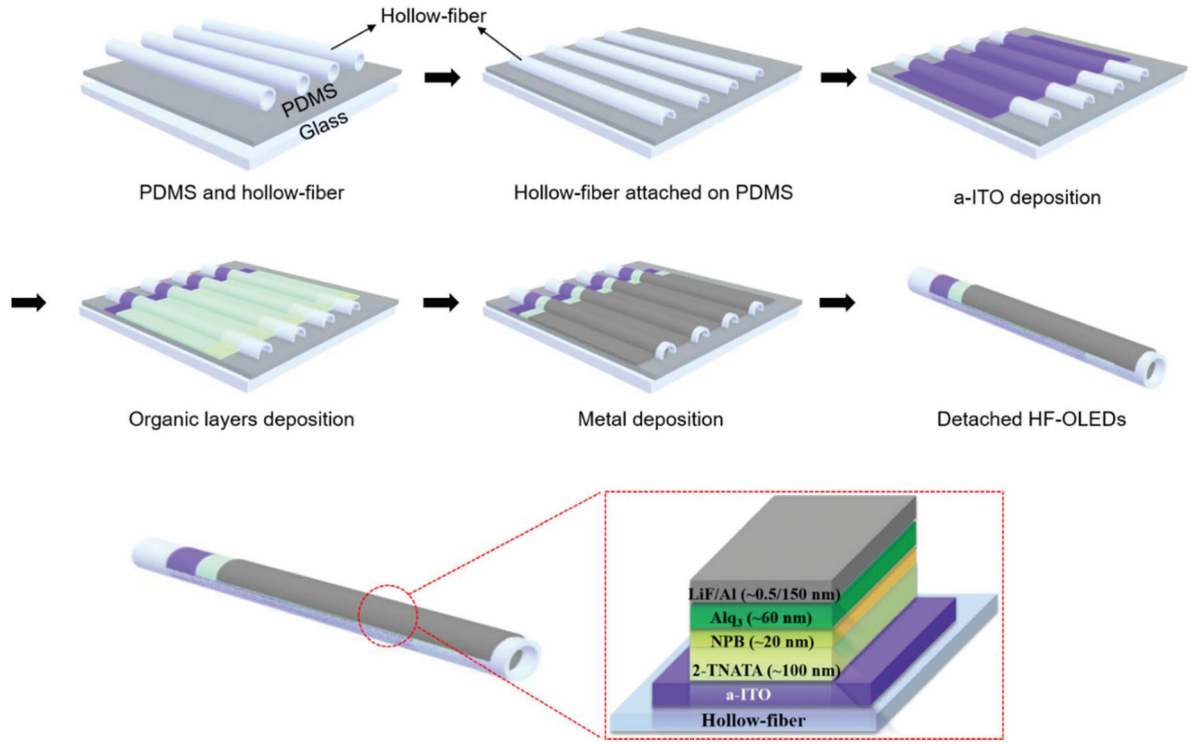

Fig. 1 Schematic of the fabrication process of the HF-OLED.

coupled power, and angular pattern of the planar- and HF-OLEDs. The refractive index values at the central wavelength (λ_c = 530 nm) of the OLED emission for glass, ITO, and organic layer were taken from the literature.[22] The geometrical designs of planar- and HF-OLEDs for the simulation are depicted in Fig. S1.† A rectangular volume source, 5 mm × 2.35 mm × 1 μm in dimension, was used as a light source. The light source was placed inside each organic layer of both planar- and HF-OLEDs. It is noteworthy that in the HF-OLED, the light source was deformed along the curvature of the HF-OLED. A number of 5 000 000 rays were used to achieve stable results. The ray polarization, ray splitting, and scattering are also considered in obtaining the nearly exact outputs. A hemispherical detector was used for the angular distribution, and the number of radial pixels and angular pixels were 180 and 46, respectively. In addition to ray-tracing simulation, wave analysis based on 2D finite-difference time-domain (FDTD) by using commercial software (RSoft CAD, Synopsys, USA) was utilized to investigate the optical phenomena in thin layers such as ITO, organic, and Al layers. The overall simulation domain were 100 μm × 50 μm in x and z directions (Fig. 7S and 8S†). The boundary condition was defined as a perfectly matched layer (PML) to absorb all the outgoing radiation. The mesh size was set to be 20 nm in the domain representing the thin layers and 40 nm for the rest of the domains. The single point source with the wavelength of 530 nm was used as a light source located at the center of organic layers. The oscillation direction of point source was considered in 3-axes such as x-, y-, and z-directions (*i.e.*, different polarizations). For better understanding the wave-guided mode, the magnified electric fields (100 μm × 5 μm) of planar-/HF-OLEDs are shown in Fig. 4(f). The magnified areas include bulk glass/ITO (150 nm)/organic layers (180 nm)/Al (150 nm). The output powers were detected by monitor located at 50 μm in z-direction. The optical constants of all materials were used with the same values with the values used in ray-tracing simulation.

Results and discussion

Fig. 2(a) visualizes the structural geometry and physical dimensions of the HF-electrode embedded substrate (PDMS film/hollow-fiber/a-ITO). The bottom hemisphere of the hollow-fiber was embedded in the PDMS film and the a-ITO layer was only deposited on the top hemisphere of the hollow-fiber. Meanwhile, Fig. 2(b) depicts the cross-sectional micrographs of the HF-electrode, taken at six different positions on the top hemisphere of the electrode, represented by different angles, *i.e.* ±90°, −60°, −30°, 0°, +30° and +60°. The external and internal diameters of the hollow-fiber were measured to be ~1.5 mm and ~1.0 mm, respectively. Therefore, the thickness of the plain hollow-fiber glass is approximately ~0.25 mm.

The thickness of the a-ITO layer, measured from the FE-SEM images, varied accordingly with the position on the curved surface of the HF-electrode, as presented in Fig. 2(a). At an angle of 0° (the top surface of HF electrode), the thickness of a-ITO was the highest (~160 nm). However, there is a corresponding reduction in the thickness of a-ITO with an increase

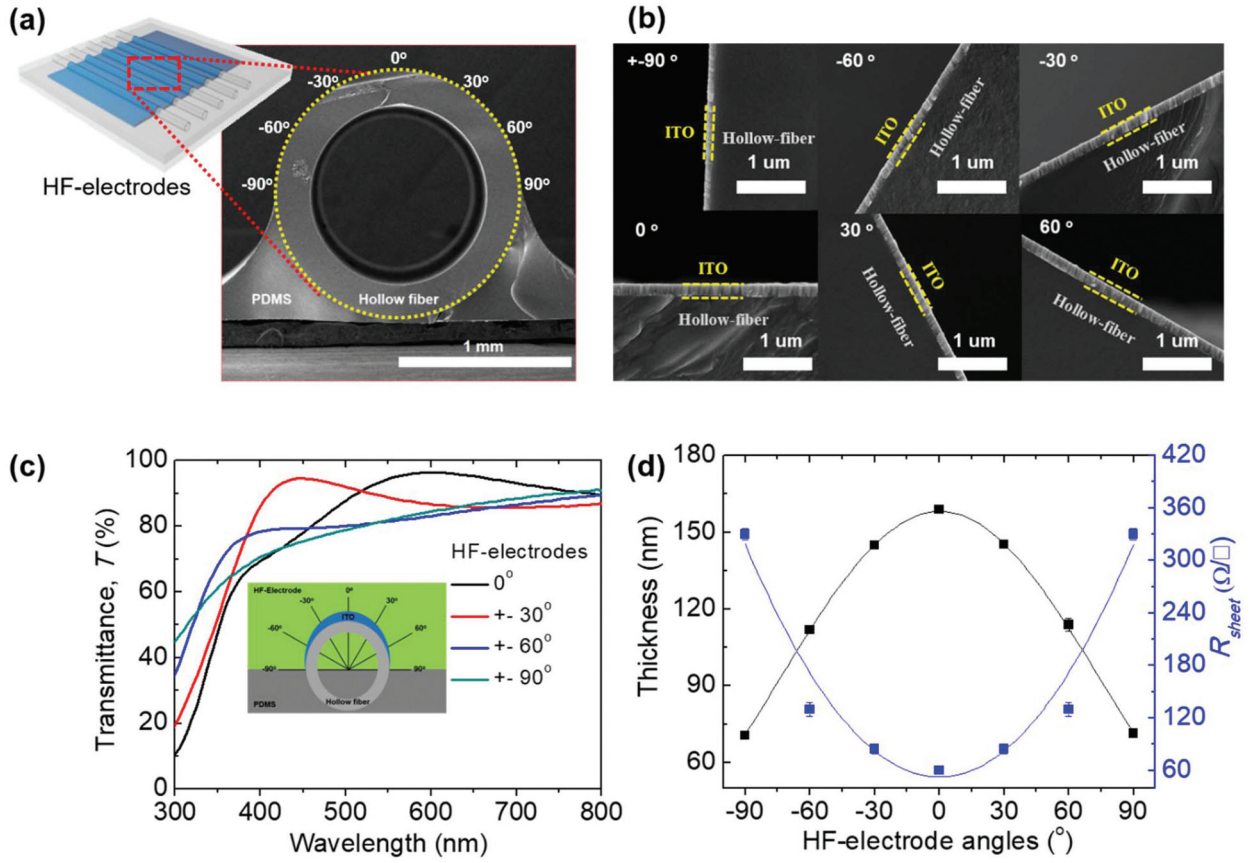

Fig. 2 (a) Low-resolution cross-sectional, (b) high-resolution cross-sectional FE-SEM micrographs of the HF-electrodes, (c) transmittance spectra of the HF-electrodes and (d) thickness and R_{sheet} of the HF-electrodes *versus* angle.

in the angle, in which it was reduced to ~70 nm at an angle of ±90° (the side of the HF electrode). The variation of the a-ITO thickness results in considerable changes in the T and R_{sheet} of the electrode. To further investigate this, the effective thickness, T and R_{sheet} of an a-ITO layer on an HF electrode were investigated as a function of angle (position). For these measurements, a-ITO was deposited on flat glass substrate with an actual thickness of a-ITO corresponding to each analyzed angle of the HF-electrode. Fig. 2(d) clearly shows that there is an inverse relationship between the R_{sheet} and the effective thickness of the a-ITO electrode. Specifically, the a-ITO electrode exhibits an R_{sheet} as low as (60 ± 3) Ω □$^{-1}$ at an angle of 0°. However, the R_{sheet} of the HF-electrode increases to (330 ± 7) Ω □$^{-1}$ at an angle of ±90°, corresponding to ~70 nm-thick a-ITO. Apparently, a ~2.3 times reduction in the effective thickness of a-ITO electrode has led to a corresponding ~5.5 times higher R_{sheet}. The exponential increase in the R_{sheet} of a-ITO electrode at lower thickness observed herein is believed to arise from the reduced carrier mobility in the film.[8,23,24]

Simultaneously, to a certain extent, the thickness variation also exerts an effect on the optical transmittance of the a-ITO film. Fig. 2(c) displays the transmittance spectra of a-ITO obtained at different angles of the HF-electrode, with the thickness of a-ITO ranging from 70–160 nm. When the HF electrode angle varied from 0° to 90° (reduction of film thickness), it was found that the transmittance of a-ITO films decreased, especially in the visible region (<80%), and the transmittance threshold gradually blue-shifted to a shorter wavelength. The average transmittance, T_{avg}, of the a-ITO electrode from 350–750 nm was recorded at ~83% with a variation of R_{sheet} from 60 to 330 Ω □$^{-1}$, as depicted in Fig. S2.†

Fig. 3(a) presents the current density–voltage–luminance (J–V–L) characteristics of planar-OLED and HF-OLED devices. Both devices exhibited a turn-on voltage of 3–3.5 V and reasonably operate up to ~13 V. However, the HF-OLED shows a relatively lower current density than that of the planar OLED. This finding is attributable to the less uniform thickness of an a-ITO electrode (70–160 nm), which varies with an angular dependence, as evidenced by the higher leakage current (Fig. S4†). Although the electrical characteristics do not differ materially between the HF-OLED and planar-OLED, their emission characteristics differ substantially, due to the undesirable light-extraction effects of the typical OLED.[25] Comparatively, the luminance of the HF-OLED was tremendously higher than that of planar-OLED. This result indicates that the performance of the HF-OLED is superior to that of the planar OLED and it meets the luminance requirements (500–1000 cd m^{-2})

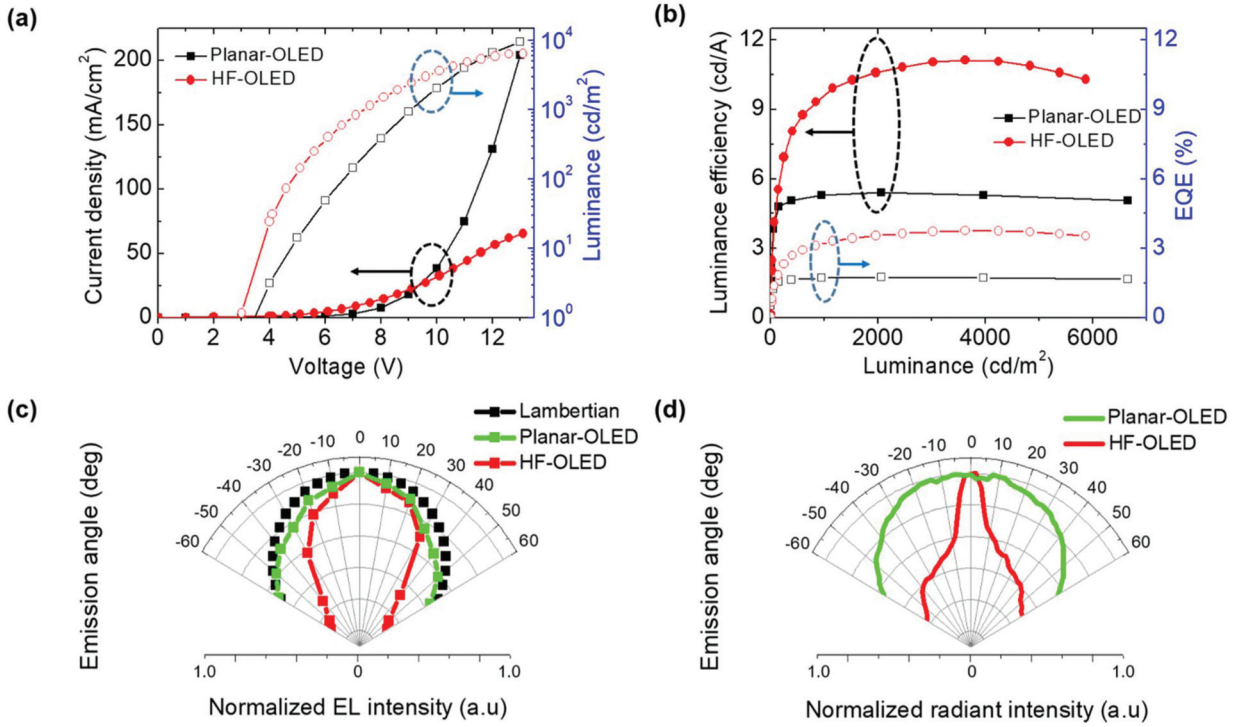

Fig. 3 (a) Current density–voltage–luminance characteristics and (b) luminance efficiency-luminance-external quantum efficiency characteristics of the planar- and HF-OLEDs. (c) Angular EL intensity profile and (d) simulated radiant intensity profile of the planar and HF-OLED at different angles.

for mobile or wearable display applications.[26,27] However, at high voltages, especially over 11 V, the maximum luminance of planar OLED and the HF-OLED devices were recorded as ~9500 and ~6300 cd m^{-2}, respectively. The disparity observed in the highest luminance value between the planar-OLED and HF-OLED device primarily arises from the angle-resolved thickness uniformity and the R_{sheet} of a-ITO electrode. Owing to the circular geometry of hollow-fiber, the a-ITO electrode on HF-OLED exhibited less thickness uniformity and higher R_{sheet} at certain substrate angles, thereby increased the series resistance of the device. Consequently, the maximum luminance of HF-OLED is lower than that of planar-OLED. A similar finding has also been reported previously in the work of Kwon *et al.*[8]

Fig. 3(b) shows that the LE and EQE *versus* luminance characteristics of the planar-OLED and HF-OLED devices. The maximum LE of the planar- and HF-OLED were ~5.0 and ~11.0 cd A^{-1}, respectively. In comparison with other fiber-shaped OLEDs with similar device architecture, the HF-OLED device fabricated herein exhibited an unprecedentedly high luminance efficiency of over 10 cd A^{-1}, which is currently the highest value ever reported and greatly exceeds that of a planar counterpart reported in the literature (5–6 cd A^{-1}),[28–33] as presented in Table S1.†

Furthermore, the Lambertian emission distribution, normalized angular emission profile, and the electroluminescence spectra of the HF-OLED were investigated, as displayed in Fig. 3(c). There is no visible wavelength shift in the EL peak position for the HF-OLED when light is captured under different viewing angles from −60° to 60° (Fig. S5†). Due to the hollow-fiber geometry, the HF-OLED exhibits highly unique angular profiles in the zenith (φ) direction. This finding predominantly arises from the thickness variation of the a-ITO electrode at different angles. In particular, the HF-OLED displayed stronger emission at a very narrow angle in the φ direction, because the thick ITO electrode covers the upper hemisphere of the cylindrically-shaped fiber, and light is trapped and propagates inside the fiber substrate. At an angle of 0° (the top surface of hollow-fiber), the HF-OLED displayed the strongest EL emission, resulting from its cylindrical geometry and the highest a-ITO/organic layer thickness. At emission angles over 30°, the detected EL emissions from the HF-OLED mainly arises from the extraction of the light propagated inside the hollow-fibers,[7] and there is therefore a corresponding reduction of the EL intensity with an increase in the emission angle.

On the other hand, the angular emission profile of the planar-OLED is fairly normal and consistent, showing only minor deviations in the EL intensity from the Lambertion emission, up to an angle of 60°. Based on a full trans-scale optical simulation, the light out-coupling pathways of the HF-OLED were visualized (Fig. S6†) and the radiant intensities of the planar-and HF-OLED at different angles were simulated and compared, as shown in Fig. 3(d). In comparison with the consistent radiant intensity of the planar-OLED, the normalized radiant intensity of the HF-OLED appears to be highly angle-dependent. With an increase of the tilting angle, the

radiant intensity of the HF-OLED deteriorated rapidly, due to the reduction of effective a-ITO/organic layer thickness. The simulated radiant intensity profiles of the planar- and HF-OLED are in good agreement with their experimental normalized angular emission profiles, as seen in Fig. 3(d).

In addition, the total EQE (EQE_{tot}) of the planar- and HF-OLED devices were measured using an integrating sphere and the related results are shown in Fig. 4(a). The calculation of the EQE was based on the collection of light power from a direction normal to the device whereas for the calculation of EQE_{tot}, all of the scattered light power in the surrounding of the device was taken into account.[34] The maximum EQE_{tot} of the HF-OLED was recorded at 4.60%, which is more than ~2.0 times higher than that of the planar-OLED (2.25%). The improvement in EQE_{tot} directly contributes to the luminance efficiency of the device. As commonly accepted, it is challenging to improve light extraction in a planar-OLED structure without the use of an internal/external out-coupling medium.[34,35] However, the utilization of a cylindrically shaped hollow-fiber substrate, which simultaneously functions as a refractive index-matching material as well as an out-coupling lens, could significantly improve light scattering and couple the substrate wave-guided modes to the output. Simultaneously, the thickness of hollow-fiber substrate (~0.5 mm) is lower than that of glass substrate (~0.7 mm), which is beneficial in helping to suppress substrate mode light loss and directly improved the light extraction efficiency of HF-OLED.[36]

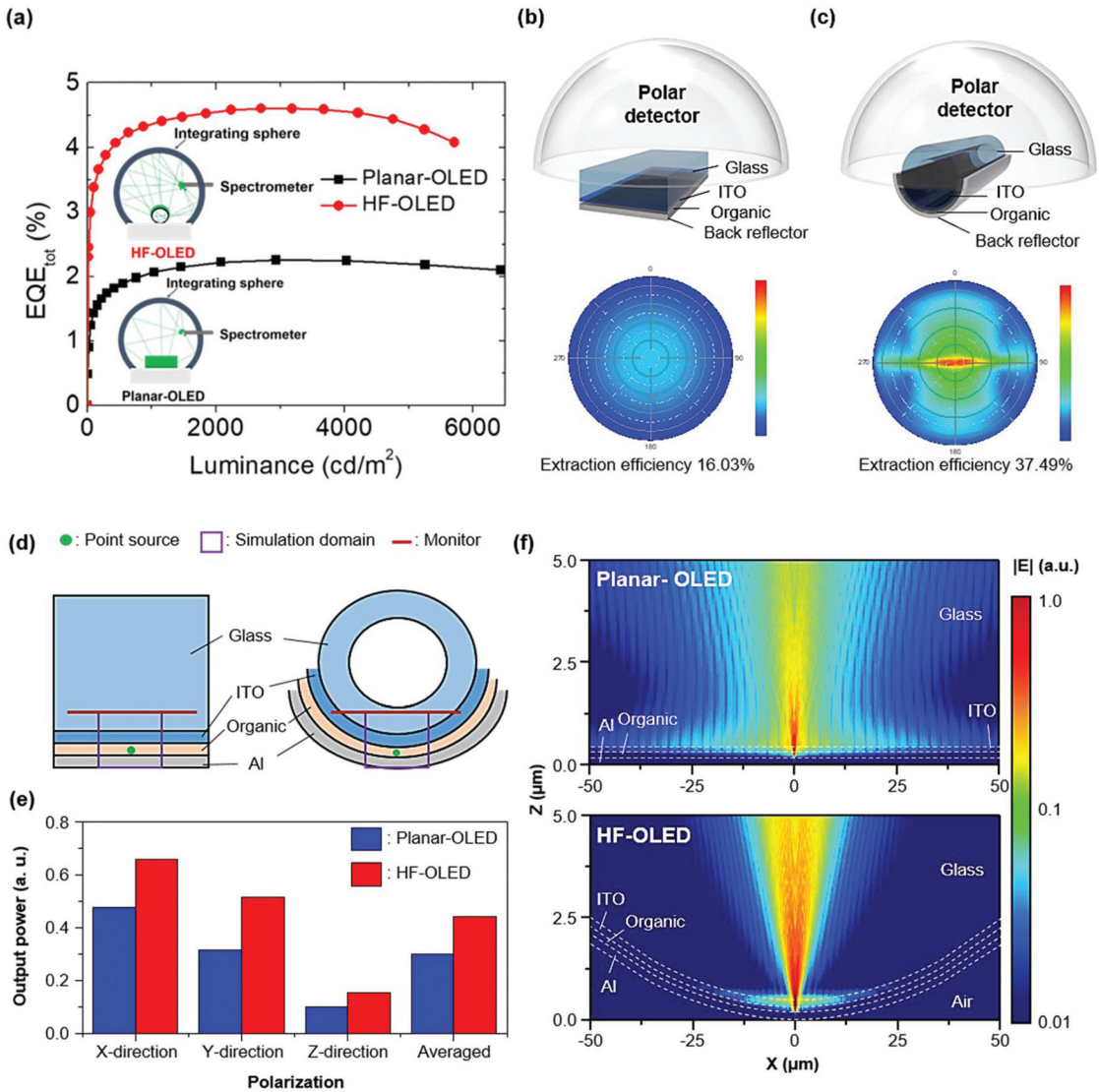

Fig. 4 (a) Total EQE *versus* luminance for the planar and HF-OLED, a schematic illustration of optical simulation based Monte Carlo methods of (b) the planar OLED and (c) HF-OLED, where the dimensions of the device structure are not drawn to scale. (d) Schematic illustrations of 2D FDTD simulation domain for flat and HF-OLEDs. (e) The output power values captured by the monitor in both devices at steady state. 3-axes oscillated dipole source was calculated. 'Averaged' indicates that the averaged value of 3-axes oscillated dipole sources. (f) Electric field distributions of flat and HF-OLEDs in the magnified area (100 μm × 5 μm). The overall simulation domain (100 μm × 50 μm) is shown in Fig. S7 and S8.†

To understand and further verify the role of the hollow-fiber in the operational mechanisms of the OLED, a full trans-scale optical simulation was conducted. The simulation result reflects that the light extraction efficiency of the HF-OLED (37.49%) is remarkably higher than that of the planar-OLED (16.03%), as shown in Fig. 4(b) and (c). This is evidenced by the tremendously higher radiant intensity of the HF-OLED *versus* the planar OLED at all angles, especially at 0° (the top surface of the HF-electrode), due to the light extraction from the substrate mode. As a result, the light extraction efficiency of the HF-OLED is about 2.3 times higher than of a planar-OLED. Fig. 4(d)–(f) demonstrate that the layout of hollow-fiber can extract the confined light of wave-guided mode. The output powers captured by monitor are different depending on the polarization of dipole source, but the powers of HF-OLED are much higher than those of planar-OLED (Fig. 4(e) and Fig. S7†). The wave-guided mode in ITO layer is widely observed in planar-OLED, whereas the HF-OLED shows a weak light localization in ITO layer and the strong light propagation in z direction (Fig. 4(f)). The total electric field distributions are shown in Fig. S8.† These simulation outcomes here substantiates our claim that the use of a hollow-fiber substrate can effectively suppress wave-guided mode. Apparently, the use of a hollow-fiber substrate is capable of addressing the common light out-coupling issues experienced by the planar OLED and directly contributes to the luminance improvement of the OLED device. The light extraction efficiency improvement observed herein agrees well with the EQE_{tot} improvement discussed previously, indicating that the simulated results yield a quantitative agreement with the experimental values.

The HF-OLED also exhibits a novel color-tunable nature, which is an important criterion to fulfill in a modern lighting application. Typically, the emission color of planar-OLEDs can be obtained *via* varying the emitter materials, *i.e.* mixing either three primary colors (red, green, blue) or two complementary colors for down-conversion methods,[37–39] and doping methods.[19,40,41,44] However, for the fiber-shaped OLED, color variety can be realized by assembling two or more OLED devices that emit different colors, whereby the luminance of each device can be continuously or independently tuned by varying the external current cource.[6] Herein, we successfully modulated the emission color of the HF-OLED from green to yellowish-green without the need to assemble separate devices. This was executed by injecting a super-yellow solution into the empty core of the hollow-fiber. The super-yellow solution was prepared by dissolving an as-bought super-yellow, light-emitting PPV copolymer (Merck, PDY-132) in toluene, at a concentration of 5 mg ml^{-1}.

In the pristine state, the as-fabricated HF-OLED exhibited dominant luminance and EL emission intensity in the green band with a peak position of 518 nm, as displayed in Fig. 5(a). On the other hand, after injecting super-yellow solution (PL peak position ~546 nm), the emission of HF-OLED turns yellowish-green (Fig. 5(c)) and its EL peak position was red-shifted to 531 nm. Fascinatingly, the full width half-maximum (FWHM) values of EL emission of the yellowish-green HF-OLED (67 nm) is much narrower than that of the pristine HF-OLED (113 nm), indicating an improved color-purity of the OLED device.[42] This finding can be attributed to the presence of SY solution on the external structure of HF-OLED, which has an absorption range (~300–540 nm)[43] relatively close to the emission range of HF-OLED (~460–750 nm), as displayed in Fig. S9.† In this context, the color-tuning mechanism of HF-OLED can be explained in two steps, namely (i) initial green emission from the NPB/Alq_3 emissive layer in HF-OLED device and (ii) partial absorption of green emission and subsequent conversion to yellowish-green emission by the external SY solution. This claim is evidenced by the narrower FWHM and quenching in the EL emission (Fig. S9†) of HF-OLED after SY solution-injection. On another note, there is only marginal wavelength shift in the emission spectra of HF-OLED after solution-injection because the SY solution existed as an external fluorescent medium and therefore, it has negligible influence on the intrinsic optical energy band alignment of HF-OLED device. Based on the CIE 1931 standard color-matching functions, the green EL emission for the pristine HF-OLED and yellow PL emission of the super-yellow solution have been represented in (x, y) chromaticity coordinates, which are (0.34,

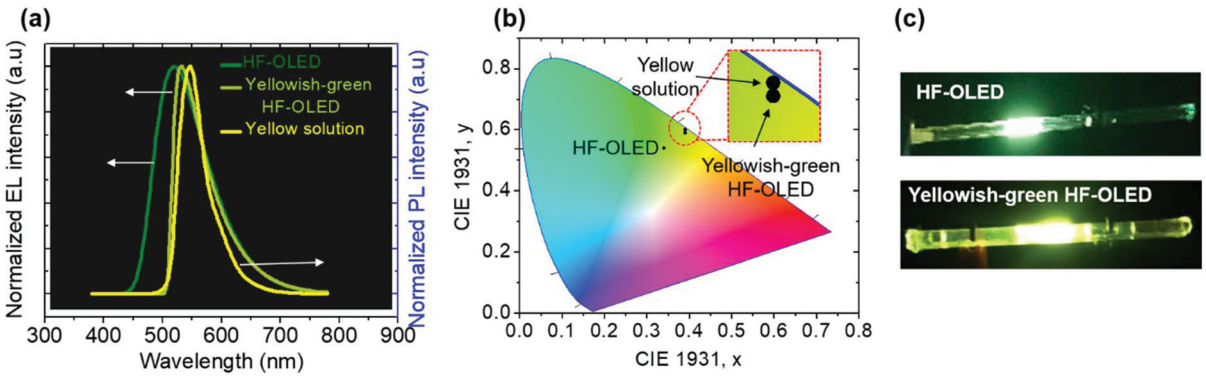

Fig. 5 (a) Normalized EL spectra of green/yellowish-green HF-OLED and normalized PL spectrum of super-yellow solution, (b) CIE spectra of green/yellowish-green HF-OLED and super-yellow solution and (c) photography of green/yellowish-green HF-OLED.

0.54) and (0.39, 0.59) respectively. Meanwhile, the chromaticity coordinate of the yellowish-green emission of the HF-OLED after the solution injection was recorded at (0.40, 0.60), as depicted in Fig. 5(b). The novel device geometry and color-tunable nature of the HF-OLED is potentially of interest for use in display and lighting applications, as well as in fiber-optic photonic devices.

Conclusion

In summary, we demonstrated the unprecedented use of a novel hollow-fiber substrate in the fabrication of a high luminance, cylindrically-shaped OLED, using a novel hollow-fiber electrode. The as-fabricated HF-OLED device exhibited more than a two-fold higher EQE_{tot} (~4.60%) as compared with that of the planar OLED device (~2.25%). The outcomes of optical simulations also yielded a very good quantitative agreement with the experimental result, revealing that the cylindrical geometry of a hollow-fiber electrode can enhance the propagation of light and simultaneously function as a refractive index matching material to suppress wave-guided mode light loss. Additionally, the as-fabricated HF-OLED device displayed facile color-tunability, in which its EL emission was successfully modulated from a green to yellow-green band simply *via* injection of a colored solution into the empty core of the hollow-fiber. The unorthodox geometry and emission properties of the HF-OLED could find useful applications in modern lighting and next-generation optoelectronic devices.

Conflicts of interest

There are no conflicts to declare.

Acknowledgements

This work was financially supported by the Pioneer Research Center Program (NRF-2013M3C1A3065528), by the Basic Science Research Program (NRF-2017R1A2B2001838) and by Creative Materials Discovery Program (NRF-2017M3D1A1039288) through the National Research Foundation (NRF) of Korea, funded by the Ministry of Science, ICT & Future Planning.

References

1 W. Zeng, L. Shu, Q. Li, S. Chen, F. Wang and X. M. Tao, *Adv. Mater.*, 2014, **26**, 5310–5336.
2 J. Liang, L. Li, X. Niu, Z. Yu and Q. Pei, *Nat. Photonics*, 2013, **7**, 817–824.
3 M. Bayandir, F. Sorin, A. F. Abouraddy, J. Viens, S. D. Hart, J. D. Joannopoulos and Y. Fink, *Nature*, 2004, **431**, 826–829.
4 O. Shapira, K. Kuriki, N. D. Orf, A. F. Abouraddy, G. Benoit, F. Viens, A. Rodriguez, M. Ibanescu, J. D. Joannopoulos, Y. Fink and M. M. Brewster, *Opt. Express*, 2006, **14**, 1921–1923.
5 E. Ghadiri, N. Taghavinia, S. M. Zakeeruddin, M. Grätzel and J.-E. Moser, *Nano Lett.*, 2010, **10**, 1632–1638.
6 Z. Zhang, K. Guo, Y. Li, X. Li, G. Guan, H. Li, Y. Luo, F. Zhao, Q. Zhang, B. Wei, Q. Pei and H. Peng, *Nat. Photonics*, 2015, **9**, 233–238.
7 S. Kwon, W. Kim, H. Kim, S. Choi, B. C. Park, S. H. Kang and K. C. Choi, *Adv. Electron. Mater.*, 2015, **1**, 1–8.
8 S. Kwon, H. Kim, S. Choi, E. G. Jeong, D. Kim, S. Lee, H. S. Lee, Y. C. Seo and K. C. Choi, *Nano Lett.*, 2018, **18**, 347–356.
9 B. O'Connor, K. H. An, Y. Zhao, K. P. Pipe and M. Shtein, *Adv. Mater.*, 2007, **19**, 3897–3900.
10 M.-C. Oh, J.-H. Park, H. J. Jeon and J. S. Go, *Displays*, 2015, **37**, 72–78.
11 Y. Qu, J. Kim, C. Coburn and S. R. Forrest, *ACS Photonics*, 2018, **5**, 2453–2458.
12 S. Möller and S. R. Forrest, *J. Appl. Phys.*, 2002, **91**, 3324–3327.
13 S.-R. Shin, H. B. Lee, W.-Y. Jin, K.-J. Ko, S. Park, S. Yoo and J.-W. Kang, *J. Mater. Chem. C*, 2018, **6**, 5444–5452.
14 B. Liu, L. Wang, M. Xu, H. Tao, D. Gao, J. Zou, L. Lan, H. Ning, J. Peng and Y. Cao, *J. Mater. Chem. C*, 2014, **2**, 9836–9841.
15 J. M. Lupton, B. J. Matterson, I. D. W. Samuel, M. J. Jory and W. L. Barnes, *Appl. Phys. Lett.*, 2000, **77**, 3340–3342.
16 Y. J. Lee, S. H. Kim, J. Huh, G. H. Kim, Y. H. Lee, S. H. Cho, Y. C. Kim and Y. R. Do, *Appl. Phys. Lett.*, 2003, **82**, 3779–3781.
17 Y. H. Kim, C. Wolf, H. Cho, S. H. Jeong and T. W. Lee, *Adv. Mater.*, 2016, **28**, 734–741.
18 D. Luo, Q. Chen, Y. Gao, M. Zhang and B. Liu, *ACS Energy Lett.*, 2018, **3**, 1531–1538.
19 B. Liu, X. L. Li, H. Tao, J. Zou, M. Xu, L. Wang, J. Peng and Y. Cao, *J. Mater. Chem. C*, 2017, **5**, 7668–7683.
20 Z. Zhang, Q. Zhang, K. Guo, Y. Li, X. Li, L. Wang, Y. Luo, H. Li, Y. Zhang, G. Guan, B. Wei, X. Zhu and H. Peng, *J. Mater. Chem. C*, 2015, **3**, 5621–5624.
21 R. Y. Rubinstein and D. P. Kroese, *Simulation and the Monte Carlo Method*, Wiley, 3rd edn, 2016, ISBN: 978-1-118-63216-1.
22 M. J. Park, G. H. Kim, Y. H. Son, H. W. Bae, J. H. Kong and J. H. Kwon, *Opt. Express*, 2014, **22**, 19919.
23 J. H. Kim, T. Y. Seong, K. J. Ahn, K. B. Chung, H. J. Seok, H. J. Seo and H. K. Kim, *Appl. Surf. Sci.*, 2018, **440**, 1211–1218.
24 A. P. Amalathas and M. M. Alkaisi, *J. Mater. Sci.: Mater. Electron.*, 2016, **27**, 11064–11071.
25 C. F. Madigan, M.-H. Lu and J. C. Sturm, *Appl. Phys. Lett.*, 2000, **76**, 1650–1652.
26 S. Steudel, K. Myny, S. Schols, P. Vicca, S. Smout, A. Tripathi, B. Van Der Putten, J. L. Van Der Steen, M. Van Neer, F. Schütze, O. R. Hild, E. Van Veenendaal, P. Van Lieshout, M. Van Mil, J. Genoe, G. Gelinck and P. Heremans, *Org. Electron. Phys. Mater. Appl.*, 2012, **13**, 1729–1735.

27 M. S. White, M. Kaltenbrunner, E. D. Głowacki, K. Gutnichenko, G. Kettlgruber, I. Graz, S. Aazou, C. Ulbricht, D. A. M. Egbe, M. C. Miron, Z. Major, M. C. Scharber, T. Sekitani, T. Someya, S. Bauer and N. S. Sariciftci, *Nat. Photonics*, 2013, **7**, 811–816.
28 D. Ma, C. S. Lee, S. T. Lee and L. S. Hung, *Appl. Phys. Lett.*, 2002, **80**, 3641–3643.
29 Y. Q. Li, J. X. Tang, Z. Y. Xie, L. S. Hung and S. S. Lau, *Chem. Phys. Lett.*, 2004, **386**, 128–131.
30 L. Zhou, J. Y. Zhuang, M. S. Song, W. M. Su and Z. Cui, *J. Phys. D: Appl. Phys.*, 2014, **47**, 115504.
31 C. Cheng, Y. Chu and F. Chang, *Nano Energy*, 2015, **13**, 1–8.
32 C.-H. Shin, E. Y. Shin, M.-H. Kim, J.-H. Lee and Y. Choi, *Opt. Express*, 2015, **23**, A133.
33 H.-W. Lu, C.-W. Huang, P.-C. Kao, S.-Y. Chu and Y.-D. Juang, *ECS J. Solid State Sci. Technol.*, 2015, **4**, R54–R59.
34 J.-W. Shin, D.-H. Cho, J. Moon, C. W. Joo, J. Lee, J. W. Huh, S. K. Park, J.-H. Han, N. S. Cho, J. Hwang, H. Y. Chu and J.-I. Lee, *Opt. Lett.*, 2014, **39**, 3527.
35 I. Lee, J. Y. Park, S. Gim, J. Ham, J. H. Son and J. L. Lee, *Small*, 2015, **11**, 4480–4484.
36 K. Saxena, V. K. Jain and D. S. Mehta, *Opt. Mater.*, 2009, **32**, 221–233.
37 P. E. Burrows, S. R. Forrest, S. P. Sibley and M. E. Thompson, *Appl. Phys. Lett.*, 1996, **69**, 2959–2961.
38 Z. Shen, *Science*, 1997, **276**, 2009–2011.
39 D. Song, I.-J. Bae, A. K. Srivastava, M. Kim, B.-J. Lee, J.-K. Shin and J.-W. Kang, *Mol. Cryst. Liq. Cryst.*, 2016, **636**, 52–59.
40 B. Liu, H. Tao, L. Wang, D. Gao, W. Liu, J. Zou, M. Xu, H. Ning, J. Peng and Y. Cao, *Nano Energy*, 2016, **26**, 26–36.
41 B. Liu, H. Nie, G. Lin, S. Hu, D. Gao, J. Zou, M. Xu, L. Wang, Z. Zhao, H. Ning, J. Peng, Y. Cao and B. Z. Tang, *ACS Appl. Mater. Interfaces*, 2017, **9**, 34162–34171.
42 X. Dai, Y. Deng, X. Peng and Y. Jin, *Adv. Mater.*, 2017, **29**, 1607022.
43 M. Bajpai, K. Kumari, R. Srivastava, M. N. Kamalasanan, R. S. Tiwari and S. Chand, *Solid State Commun.*, 2010, **150**, 581–584.
44 T.-H. Han, M.-R. Choi, C.-W. Jeon, Y.-H. Kim, S.-K. Kwon and T.-W. Lee, *Sci. Adv.*, 2016, **2**, e1601428.

